

Optical identifications and spectroscopy of a faint radio source sample: the nature of the sub-mJy population^{*}

C. Gruppioni¹, M. Mignoli² & G. Zamorani^{2,3}

¹ *Imperial College of Science, Technology and Medicine, Prince Consort Road, London SW7 2BZ, U.K.*

² *Osservatorio Astronomico di Bologna, via Zamboni 33, I-40126 Bologna, Italy*

³ *Istituto di Radioastronomia del CNR, via Gobetti 101, I-40129 Bologna, Italy*

e-mail: c.gruppioni@ic.ac.uk

Accepted 1998 November 18. Received 1998 September 24

ABSTRACT

Deep imaging and spectroscopy have been carried out for optical counterparts of a sample of 68 faint radio sources ($S > 0.2$ mJy) in the “Marano Field”. About 60% of the sources have been optically identified on deep CCD exposures (limit $R \simeq 24.0$) or ESO 3.6-m plates (limit $b_J \simeq 22.5$). Thirty-four spectra (50% of the total radio sample) were obtained with the ESO 3.6-m telescope and 30 redshifts were determined. In addition to a few broad line active galactic nuclei, three main spectroscopic classes have been found to dominate the faint radio galaxy population: (1) Early-type galaxies (without emission-lines in their spectra) having $0.1 < z < 0.8$ and covering the range of radio fluxes 0.2 – 30 mJy. (2) Late-type galaxies (with narrow emission-lines in their spectra) at moderate redshift ($z < 0.4$), with relatively bright magnitudes ($B < 22.5$) and sub-milliJanski radio fluxes. When applicable, the diagnostic diagrams for these sources are consistent with the lines being produced by star-formation activity. (3) A group of bright high-redshift ($z > 0.8$) radio galaxies with moderate-to-strong [OII] emission. All of them have $B > 22.5$ and most of them have $S_{1.4\text{ GHz}} > 1$ mJy. They have spectra, colours and absolute magnitudes similar to those of the classical bright elliptical radio galaxies found in surveys carried out at higher radio fluxes. Star-forming galaxies do not constitute the main population of our radio sources identified with galaxies. In fact, even at sub-mJy level the majority of our radio sources are identified with early-type galaxies. This apparent discrepancy with previous results is due to the fainter magnitude limit reached in our spectroscopic identifications. Moreover, using mainly the large radio-to-optical ratio and the information from the available limits on the optical magnitudes of the unidentified radio sources, we conclude that the great majority of them are likely to be early-type galaxies, at $z > 1$. If correct, it would suggest that the evolution of the radio luminosity function of spiral galaxies, including starbursts, might not be as strong as suggested in previous evolutionary models.

Key words: galaxies: active – galaxies: starburst – cosmology: observations – radio continuum: galaxies.

1 INTRODUCTION

In the last decade, deep radio surveys (Condon & Mitchell 1984; Windhorst 1984; Windhorst et al. 1985) have pointed out the presence of a new population of radio sources appearing below a few mJy and responsible for the observed flattening in the differential source counts (normalized to Euclidean ones). Several scenarios have been developed to interpret

this “excess” in the number of faint radio sources, invoking a non-evolving population of local ($z < 0.1$) low-luminosity galaxies (Wall et al. 1986), strongly-evolving normal spirals (Condon 1984, 1989) and actively star-forming galaxies (Windhorst et al. 1985, 1987; Danese et al. 1987; Rowan-Robinson et al. 1993). The latter scenario is supported by the existing optical identification works performed for the sub-mJy population. These works have, in fact, shown that the sub-mJy sources are mainly identified with faint blue galaxies (Kron, Koo & Windhorst 1985; Thuan & Condon 1987), often showing peculiar optical morphologies indica-

^{*} Based on observations collected at the European Southern Observatory, LaSilla, Chile

tive of interaction and merging phenomena and spectra similar to those of the star-forming galaxies detected by IRAS (Franceschini et al. 1988; Benn et al. 1993). However, since the majority of these objects have faint optical counterparts, visible only in deep CCD exposures (down to $B \sim 24-25$), all these works are based on small percentages of identification. For example, the Benn et al. spectroscopic sample, despite the fact that it is the largest sample so far available in literature, corresponds to slightly more than 10 per cent of the total radio sample.

In order to better understand the nature of the sub-mJy radio galaxy population on the basis of a larger identification fraction than the ones obtained so far, we performed deep photometric and spectroscopic identifications for a faint radio source sample in the “Marano Field”. Here we present the results of the identification of 68 objects, which represent the total radio sample obtained by joining together the two $S > 0.2$ mJy complete samples at 1.4 and 2.4 GHz in the “Marano Field” (see Gruppioni et al. 1997). We were able to reach a relatively high identification fraction with respect to previous works, since we optically identified 63% of the 68 radio sources and we obtained spectra for 34 of them ($\sim 50\%$ of the total sample). These constitute the highest identification fractions so far available in literature for sub-mJy radio samples.

The paper is structured as follows: in section 2 we describe the radio sample; in section 3 we present the photometric data and optical identifications; in section 4 we present the spectroscopic results, including spectral classification for the optical counterparts and notes on individual objects; in section 5 we discuss the radio and optical properties of the faint radio source population; in the last two sections we discuss our results and present our conclusions.

2 THE RADIO SAMPLE

Deep radio surveys with the Australia Telescope Compact Array (ATCA) have been carried out at 1.4 and 2.4 GHz, with a limiting flux of ~ 0.2 mJy at each frequency, in the “Marano Field” (centered at $\alpha(2000) = 03^{\text{h}} 15^{\text{m}} 09^{\text{s}}$, $\delta(2000) = -55^{\circ} 13' 57''$), for which deep optical and X-ray data are also available.

The two radio samples, complete at the $5\sigma_{\text{local}}$ level, consist of 63 and 48 sources respectively at 1.4 and 2.4 GHz. The main results of the radio data analysis are extensively described by Gruppioni et al. (1997). The 1.4 GHz differential source counts show the flattening below about 1 mJy found by previous authors (Condon & Mitchell 1984; Windhorst et al. 1985) and considered as the typical feature of the sub-mJy population. From the study of the spectral index distribution as a function of flux, a significant flattening of the spectral index toward fainter fluxes has been found for the higher frequency selected sample (2.4 GHz), while the median spectral index (α_{med}) is consistent with remaining constant at ~ 0.8 ($f_{\nu} \propto \nu^{-\alpha}$) for the sample selected at 1.4 GHz. However, at both frequencies a significant number of sources with inverted spectrum do appear at flux densities $\lesssim 2$ mJy. In particular, objects with inverted spectra constitute $\sim 13\%$ of the total 1.4 GHz sample and $\sim 25\%$ of the total 2.4 GHz one. For the latter sample this percentage increases to $\sim 40\%$ for $S < 0.6$ mJy.

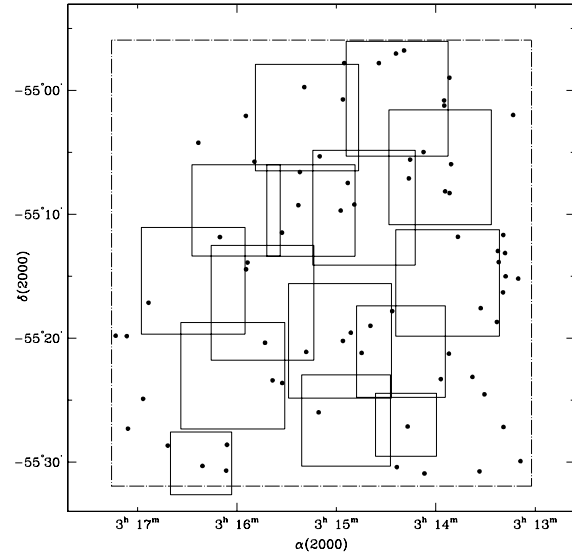


Figure 1. CCD coverage of the inner part of the “Marano Field” in the V and R bands. The area covered by the radio observations is represented by the dashed box. The filled dots are the 68 radio sources.

The total radio source sample considered in this paper for the optical identification work consists of the 1.4 GHz complete sample joined together with the 5 sources detected only at 2.4 GHz above the $5\sigma_{\text{local}}$ level.

3 PHOTOMETRY AND OPTICAL IDENTIFICATION

For the identification of our radio sources we used the photometric data already available for the “Marano Field”. These data consist of ESO 3.6-m plates in the bands U_K , J_K and F_K (Kron 1980) covering an area of ~ 0.69 sq.deg. (the plates include the entire radio field, that is ~ 0.36 sq. deg.) and reaching limit in magnitudes of $J_K \sim 22.5$ and $U_K, F_K \sim 22.0$. The data from the plates have been utilized for the selection and definition of a complete sample of faint quasars with $J \leq 22.0$, the MZZ sample (Marano, Zamorani & Zitelli 1988; Zitelli et al. 1992). Moreover, the inner part of the field ($\sim 15'$ radius) has been observed with the ESO NTT telescope, with deep CCD exposures in the U , B , V and R bands, down to limit in magnitudes $U \sim 23.5$, $B \sim 25.0$, $V \sim 24.5$ and $R \sim 24.0$. With successive observing runs a rather complete coverage of the central part of the field (corresponding to $\sim 60\%$ of the area covered by the radio observations) has been obtained in the V and R bands (see Figure 1).

A multi-colour catalog based on the deep CCD observations has been created. The images were reduced in a standard way using IRAF[†] and for the data analysis (detection,

[†] IRAF is distributed by the National Optical Astronomy Observatories, which are operated by AURA Inc. for the NSF.

photometry and star/galaxy classification) we used SExtractor (Bertin and Arnouts 1996). More details on the data reduction and analysis can be found elsewhere (Mignoli, 1997) and a full description of the catalog is in preparation. We used the CCD overlapping regions to check the photometric errors and homogeneity in the detection and morphological classification. In the B band the typical errors are ~ 0.05 mag up to $B = 23$, growing to $0.15 \div 0.20$ at the limiting magnitude of $B=25$. In the R band the error ranges from ~ 0.07 at $R = 22$ to ~ 0.20 at $R = 24$.

For the identification of the 50 radio sources which fall in the R band CCD frames, we used the magnitudes and positions of the optical sources given in the catalog. For the 18 radio sources outside the area covered by CCD frames, we used the magnitudes and positions of the optical sources taken from the plates data. In this case the U_K , J_K and F_K magnitudes of the photographic system have been transformed to U , B , V and R magnitudes of the standard Johnson/Cousin system of the CCD data, according to the transformation formulae given by Kron (1980) and Koo & Kron (1982):

$$U \approx U_K \quad \frac{V + R}{2} \approx F_K$$

$$B = J_K + 0.20(J_K - F_K)$$

$$V = F_K + 0.34(J_K - F_K)$$

The correctness of this transformation between the two photometric systems has been checked using the objects detected both in the plates and in the CCD frames: in all the four bands the average of the magnitude differences is less than 0.05 mag, implying a good consistency between the CCD and the plates photometry, whereas the scatter of the points gives an estimate of the random errors of ~ 0.10 mag for the B, V bands and of ~ 0.15 mag for the U, R bands.

A summary of the results of the optical identification and photometry for all the 68 radio sources is given in Table 1. The table is arranged as follows. The source number, their radio flux in the 1.4 and 2.4 GHz catalogs of Grupponi et al. (1997) and the radio spectral index are listed in the first five columns. The following four columns give respectively the U , B , V and R magnitudes for all the optical counterparts within 5 arcsec from the radio position. The magnitudes reported in the table followed by an asterisk (*) are those obtained by the photographic plates. There are few cases where the U and B magnitudes are missing; since the size of CCDs in these bands are smaller than in the V and R ones, the U and B CCD data do not cover the entire area covered by V and R CCD. Thus for the faintest sources, not visible on the plates, it has not been possible to measure these magnitudes. The offset (in arcsec) of the optical counterpart, its likelihood ratio and a note about the environment (D=double, GR=group or CL=cluster) are listed in the last three columns.

The likelihood ratio technique adopted for source identification is the one described by Sutherland & Saunders (1992), where the likelihood ratio (L) is simply the probability of finding the true optical counterpart in exactly the position with exactly this magnitude, relative to that of finding a similar chance background object. As probability distribution of positional errors we adopted a gaussian distribution

with standard deviation of 1.5 arcseconds. This value for σ is slightly larger than the mean radio positional errors (see Grupponi et al. 1997), so to take into account the combined effect of radio and optical positional uncertainties.

For each optical candidate we evaluated also the reliability (REL), by taking into account the presence or absence of other optical candidates for the same radio source (Sutherland & Saunders 1992). Once that L has been computed for all the optical candidates, one has to choose the best threshold value for L (L_{th}) to discriminate between spurious and real identifications. This is done by studying how the completeness (C) and reliability (R) of the identification sample vary as a function of L_{th} . The best choice for L_{th} is the value which maximizes the estimator $(C + R)/2$. For this purpose, we defined C and R as functions of L_{th} according to the formulae given by de Ruiter, Willis & Arp (1977). Since we performed our optical identifications on two different kinds of optical images (with different limiting magnitudes), we had to apply the likelihood ratio method in two separate steps for two separate sub-samples of our total identification sample. First, we computed L and REL for each optical counterpart visible on plates ($R \simeq 21.8$) within 15 arcseconds from the radio source (we chose a relatively large search radius so to obtain a significant statistics for the evaluation of L). For this “bright” sub-sample thus we computed C and R for different values of L_{th} , obtaining as best values: $L_{th} = 1.5$, $C = 95.7\%$, $R = 89.8\%$. Then we applied the same method to the optical candidates visible only on our CCD exposures, having $21.8 \lesssim R \lesssim 24$. For optical candidates fainter than $R \simeq 24$ we were not able to give any reliable estimate of L and REL , since our optical catalogue is fairly incomplete at this limit. There are four such faint optical candidates in our identification sample, all of them within 1.5 arcsec from the radio position. Also for the “fainter” identification sub-sample we found $L_{th} = 1.5$ as best choice, with corresponding $C = 89.6\%$ and $R = 82.0\%$. With this threshold we have 28 likely identifications brighter than $R \simeq 21.8$ and 8 with $21.8 \lesssim R \lesssim 24$ (plus four additional possibly good identifications with objects fainter than $R \sim 24$, too faint for a reliable determination of their likelihood ratio). The reliability (REL) of each of these optical identifications is always relatively high ($> 80\%$), except for the cases where more than one optical candidate with $L > 1.5$ is present for the same source.

As shown in the last column of Table 1, a significant fraction ($\gtrsim 35\%$) of the radio sources with reliable identification occurs in pairs or groups; moreover many of these objects show a peculiar optical morphology, suggesting an enhanced radio emission due to interaction or merging phenomena. This is in agreement with the results obtained by Kron, Koo & Windhorst (1985) and Windhorst et al. (1995) in the optical identification of sub-mJy, or even μ Jy, radio sources.

4 SPECTROSCOPY

4.1 Observations

Spectroscopic observations of 34 of the 36 optical counterparts with likelihood ratio greater than 1.5 have been carried out at ESO 3.6-m telescope. The sub-sample of these 34

Table 1. Optical Identifications

$N_{1.4}$	$N_{2.4}$	$S_{1.4}$	$S_{2.4}$	α_r	U	B	V	R	Δ	L	Envir
		(mJy)	(mJy)						($''$)		
01	01	8.28	4.86	0.97		> 22.5*		> 21.8*			
02	--	0.62	< 0.53	> 0.28		> 22.5*		> 21.8*			
03	02	26.40	26.14	0.02	19.5*	19.3*	18.0*	17.1*	1.5	58.9	GR
04	--	0.67	< 0.48	> 0.62			> 24.50	> 24.00			
05	03	0.54	0.79	-0.68			> 24.50	23.21	1.0	5.7	GR?
						> 22.5*	23.34	22.03	2.1	4.5	
06	--	0.78	0.40	1.21	17.6*	17.9*	17.0*	16.9*	2.4	28.8	
07	04	0.80	1.01	-0.42	21.4*	21.6*	21.04	20.60	3.2	1.8	
08	--	0.39	< 0.28	> 0.60	19.2*	19.9*	19.66	19.43	0.3	52.4	
09	05	1.52	2.21	-0.68	20.4*	19.8*	18.34	17.65	1.1	57.2	
--	06	< 0.32	0.46	< -0.66			> 24.50	24.60	1.4	--	
10	07	20.02	15.90	0.42			> 24.50	> 24.00			
11	--	0.49	< 0.50	> -0.03	21.6*	22.2*	21.4*	20.9*	2.8	2.2	
12	--	0.50	0.32	0.83	> 23.50	> 24.50	> 24.50	> 24.00			
13	08	0.60	0.51	0.28	19.8*	20.0*	19.1*	18.8*	0.6	71.0	
14	09	2.91	1.60	1.09		> 22.5*		> 21.8*			
15	10	158.00	95.94	0.90	19.39	19.91	19.77	19.41	1.1	40.3	
--	11	0.20	0.30	-0.72			> 24.50	> 24.00			
16	13	1.33	0.83	0.85			> 24.50	> 24.00			
17	12	3.08	1.76	1.02		23.1*	22.3*	21.7*	1.1	4.9	
18	--	0.28	< 0.20	> 0.64	21.0*	20.9*	19.7*	19.2*	1.6	44.1	D
19	14	6.27	5.31	0.30	> 23.50	> 24.50	> 24.50	> 24.00			
20	15	0.38	0.43	-0.24		> 22.5*	23.50	22.12	0.9	9.9	CL
21	16	1.02	1.00	0.04			\sim 25.0	\sim 24.0	1.0	--	
22	--	0.47	0.28	0.97	21.3*	22.2*	20.77	20.07	1.1	12.0	
23	--	0.40	< 0.24	> 0.92		> 22.5*		> 21.8*			
24	--	0.46	< 0.36	> 0.48	20.0*	20.4*	20.01	19.60	1.1	18.3	
25	17	3.30	2.68	0.38	23.75	23.72	21.98	20.85	0.5	12.3	D
					> 23.50	24.50	24.25	23.30	3.6	0.5	
					22.75	23.20	22.41	21.57	3.6	0.8	
--	18	0.20	0.33	-0.88		> 22.5*	23.85	23.72	4.8	0.0	
26	19	0.45	0.48	-0.11		23.1*	21.6*	20.05	1.2	16.9	D
27	20	2.60	1.98	0.49	20.0*	19.6*	17.81	17.10	0.5	70.0	
28	21	1.66	0.98	0.95		> 22.5*		> 21.8*			
29	--	0.62	< 0.44	> 0.61			> 24.50	> 24.00			
30	22	6.32	3.88	0.89	23.11	23.68	22.73	21.78	0.4	6.2	GR
					> 23.50	24.40	23.36	22.47	3.5	0.6	
31	23	0.92	0.52	1.05		> 22.5*	22.78	21.58	2.4	2.7	D
						> 22.5*	22.55	21.93	4.3	0.1	
32	24	0.50	0.32	0.85	> 23.50	25.30	23.80	22.50	1.7	5.8	GR
					> 23.50	> 24.50	23.75	23.15	1.5	3.3	
33	25	4.83	2.68	1.07	> 23.50	> 24.50	> 24.50	> 24.00			
34	26	0.40	0.34	0.28	> 23.50	> 24.50	> 24.50	23.50	3.1	0.6	
35	--	0.41	0.25	0.87	> 23.50	24.56	23.86	23.06	4.3	0.1	
36	27	1.17	0.75	0.80			\sim 24.5	\sim 24.3	1.4		
37	28	1.01	0.62	0.87			> 24.50	> 24.00		--	
38	30	1.25	0.71	1.02	22.50	21.85	20.35	19.32	1.8	13.3	
39	29	23.10	15.70	0.70			> 24.50	> 24.00			
40	31	0.60	0.36	0.93	> 23.50	> 24.50	> 24.50	> 24.00			
41	32	1.45	2.17	-0.73	> 23.50	> 24.50	> 24.50	23.92	2.0	3.1	
42	33	30.12	19.74	0.77	> 23.50	> 24.50	> 24.50	> 24.00			
43	34	0.42	0.32	0.47	20.73	20.58	19.30	18.60	1.4	47.1	
44	35	15.08	9.59	0.82			> 24.50	> 24.00			
45	--	0.20	0.21	-0.07	> 23.50	25.10	> 24.50	> 24.00	0.5	--	
46	--	0.50	< 0.47	> 0.11	> 23.50	> 24.50	> 24.50	> 24.00			
47	--	0.47	0.27	0.98	> 23.50	22.86	21.39	20.05	1.1	16.2	GR
					21.50	21.86	21.38	20.75	4.8	0.1	

Table 1 – continued

$N_{1.4}$	$N_{2.4}$	$S_{1.4}$	$S_{2.4}$	α_r	U	B	V	R	Δ	L	Envir
		(mJy)	(mJy)						(")		
48	36	0.54	0.34	0.82	19.01	18.98	17.96	17.40	0.6	92.6	
49	37	9.04	6.66	0.55	> 23.50	> 24.50	> 24.50	> 24.00			CL?
50	--	0.28	0.18	0.81	19.11	19.44	18.48	18.01	0.5	60.6	
51	38	0.49	0.37	0.52		> 22.5*	23.10	21.90	0.5	9.5	D
						> 22.5*	23.62	22.11	2.3	3.6	
52	39	2.06	1.40	0.70		> 22.5*	23.20	22.70	1.5	5.4	
53	40	1.54	1.79	-0.28	> 23.50	> 24.50	23.00	21.45	1.5	8.7	CL
54	41	0.91	0.68	0.53		> 22.5*		> 21.8*			
55	--	0.31	0.18	0.99	20.6*	20.4*	19.0*	18.22	1.2	38.3	D
56	42	2.38	1.87	0.44		> 22.5*		22.01	0.5	14.2	
57	43	1.71	1.07	0.85	22.69	23.14	22.81	22.09	0.9	7.9	
58	44	1.29	0.91	0.63	21.2*	21.3*	20.20	19.68	4.1	1.2	
					> 23.50	> 24.50		22.76	4.2	0.1	
					> 23.50	> 24.50	> 24.50	> 24.00			
--	45	0.15	0.33	-1.42		> 22.5*		> 21.8*			
59	--	0.38	0.30	0.43		> 22.5*		> 21.8*			
60	46	0.94	0.42	1.46	23.25	23.23	22.75	21.15	2.0	5.1	GR
--	47	< 0.28	0.31	< -0.21	22.0*	21.9*	20.5*	19.8*	3.6	2.8	
61	--	0.31	< 0.20	> 0.74	20.1*	20.8*	20.1*	19.8*	0.8	31.7	
62	48	0.45	0.41	0.19		> 22.5*		> 21.8*			
63	--	0.35	< 0.28	> 0.38	22.0*	22.2*	20.6*	20.2*	0.3	31.7	
					21.6*	20.1*	20.5*	19.5*	1.5	12.8	

sources is constituted by all the 28 objects with reliable optical counterpart on the photographic plates and by 6 of the 8 with optical counterpart on CCDs having $R \leq 23.5$.

The spectroscopic observations have been performed in two different observing runs, October 29, 30 and 31 1995, and November 12 1996, with the EFOSC1 spectrograph (Enard and Delabre, 1992). The spatial scale at the detector (RCA 512², ESO CCD #8) was 0.61 arcsec pixel⁻¹. The spectral ranges covered were usually 3600–7000 Å for the blue objects at ~ 6.3 Å/pix resolution (using the grism B300) and 6000–9200 Å for the red objects at ~ 7.7 Å/pix resolution (grism R300). In a few cases (for some bright or puzzling objects) we obtained spectra with both instrumental configuration in order to cover a larger spectral domain. The slit width was between 1.5 and 2.0 arcsec in order to optimize the balance of the fraction of object’s light within the aperture (due to seeing effects) and the sky–background contribution. Because of this relatively small size, no effort was made to achieve spectrophotometric precision. The exposure times varied from a minimum of 10 minutes for the brighter optical counterparts, to a maximum of 2 hours for the fainter ones (with R close to 23).

4.2 Data Reduction

Data reduction has been entirely performed with the NOAO “Long-slit” package in IRAF. For every observing night, a bias frame was constructed averaging ten “zero exposures” taken at the beginning and at the end of each night. The

pixel-to-pixel gains were calibrated using flat fields obtained from an internal quartz lamp. The background was removed subtracting a sky–spectrum obtained by fitting the intensities measured along the spatial direction in the column adjacent to the target position. Finally, one–dimensional spectra were obtained using an optimal extraction (Horne 1986) in order to have the maximum signal–to–noise ratio also for the fainter objects. Wavelength calibration was carried out using Helium–Argon lamps taken at the beginning and at the end of each night. From the position of the sky lines in the scientific frames, we estimated the accuracy of the wavelength calibration to be about 2 Å. During each night, two standard stars have been observed for flux-calibration purpose.

4.3 Optical Spectra and Classification

From our spectroscopic observations we were able to obtain reliable redshifts for 29 of the 34 observed optical candidates. This corresponds to $\sim 43\%$ of the original radio sample. All the 34 spectra are presented in Figure 2, together with the corresponding optical images, with superimposed the contour levels of radio emission.

The redshifts have been determined by gaussian–fitting of the emission lines and via cross–correlation for the absorption–line cases. As templates for the cross–correlation we used the templates of Kinney et al. (1996). These spectra represent a variety of galaxy spectral types — from early to late–type and starbursts — and cover a wide spectral range,

Figure 2. EFOSC1 spectra of the 34 spectroscopically observed objects. The abscissae are wavelengths in \AA , while the ordinate are monochromatic fluxes in arbitrary units. Below each spectrum, the corresponding *R* CCD image (when available, otherwise the F_K photographic plate image) is shown. Contour levels of the radio emission corresponding to 2,4,6,8,12,15,20,30,50,75,100 σ are plotted superimposed to each optical image. The size of each image is 1×1 arcmin (in a few cases, where the object was close to the limit of the CCD, only one of the two dimensions is 1 arcmin) except for # 15–10 and # 38–30, whose images are 1.5×1.5 arcmin because of the radio emission extent.

from UV to near-IR, very useful for our sample with a wide range of galaxy redshifts, up to $z \approx 1$.

The results of spectroscopic analysis are presented in Table 2, which has the following format: in the first three columns the radio source number (in both 1.4 and 2.4 GHz samples) and the R magnitude are repeated with the same convention as in Table 1. The measured redshift, whenever determined, and the list of the detected emission lines are in the following columns. In the next two columns there are the [OII] $\lambda 3727\text{\AA}$ equivalent width at rest, with associated error, followed by the 4000 \AA break index[‡]. The “spectral classification”, the “final classification” (based also on colours) and a short comment are in the last three columns. The distinction between spectroscopic types given in column 9 was based on spectra, continuum indices and visual morphologies. We divided the objects in several broad classes: Early-type galaxies (*Early*), Late-type galaxies (*Late*), AGNs, stars and unclassified objects. The classification *Late(S)* indicates galaxies in which the detected emission lines allowed some analysis of line ratios and these ratios are consistent with the lines being due to star formation. Because of the faint magnitudes and the relatively low signal-to-noise ratios of our spectra, a more detailed spectral classification was very difficult to obtain. Moreover, at this stage, a number of spectra remain unclassified. The final classification reported in column 10 is based also on colours (see next section).

A preliminary distinction between different spectroscopic classes was based on the spectral lines only. Thus, first we divided the objects into those which show only absorption lines, those which show emission lines, and those which show no spectral features at all. The ones that show only absorption lines are most likely to be early-type galaxies. For the emission-line objects we attempted a classification separating objects in which emission lines are probably produced by star-formation, from those in which an active galactic nucleus is present. Four objects have been classified as AGN: three of them have strong broad lines and unresolved optical image, so they have been classified as QSOs or type 1 AGN, while the fourth one, with only narrow lines, is likely to be a type 2 Seyfert galaxy on the basis of the lines intensity ratios. In order to produce an objective classification of the narrow emission-line objects, we tentatively used the diagnostic diagrams described by Baldwin, Phillips and Terlevich (1981) and by Rola, Terlevich and Terlevich (1997), the latter for the higher redshift sources (up to $z \approx 0.7$). Unfortunately, in a few cases, the observable spectral range accessible for high redshift galaxies makes these methods useless, and the same applies to poor S/N spectra. The five spectra allowing the use of diagnostic diagrams (i.e. showing more than one line) and falling into the HII/Starburst region (*Late(S)*) show an [OII] equivalent width at rest greater than 15 \AA , suggesting a strong star-formation. Other five galaxies clearly showing late-type spectra, for which the diagnostic diagrams could not be applied, have been classified as *Late*. They are all at relatively low redshift ($z < 0.3$) and, on average, have low [OII] equivalent widths. In a couple of cases also H α is detected. Five emission-line spectra

[‡] The 4000 \AA break index as defined by Bruzual (1983), is the ratio of the average flux density f_ν in the bands 4050–4250 \AA and 3750–3950 \AA at rest.

remained unclassified at this stage, because they could not be unambiguously classified into any of the above categories (*Early*, *Late*, AGN, etc.) on the basis of their spectra only. They are all relatively high- z (> 0.8) galaxies, whose redshift determination was mainly based on a single emission line identified with [OII] $\lambda 3727$. For their classification we used their colours, as well as their absolute magnitudes and radio luminosities (see next section).

For 5 objects, showing no obvious absorption nor emission lines in their spectra, it was not possible to determine a redshift, although for one of them (# 20–15) we assumed a redshift from nearby galaxies, which are very likely to form a cluster (see notes on individual sources reported below). Four of these objects have $R > 21.8$. Therefore, although we could determine a redshift for two objects fainter than $R = 21.8$, we can consider this magnitude as the approximate limit of our spectroscopic sample. Three of the objects for which no redshift was determined (# 05–03, # 20–15, # 51–38) are tentatively classified as *Early* on the basis of their red spectra, without prominent emission features. Instead, # 57–43, a relatively blue object with two possible emission lines in its spectrum (not identified with any obvious spectral feature), remained unclassified at this stage. The last object (# 07–04) shows an extremely blue spectrum without any distinguishable line or structure, despite the relatively good S/N. The spectrum shape, together with its inverted radio spectrum and optical colours, make it a possible BL Lacertae object.

To summarize the results of our spectral classification, we subdivided the 34 spectroscopically observed objects into the following populations:

- 12 early-type galaxies showing only absorption lines (or no detectable lines at all, but with red spectra);
- 5 late-type objects, with continua typical of evolved star population, but showing modest [OII] (and eventually H α +NII) emission lines;
- 5 star-forming emission line galaxies with more than one line in their spectra and $W([\text{OII}]) > 15 \text{\AA}$;
- 5 Active Galactic Nuclei, consisting of 3 broad-line QSOs, 1 Seyfert 2 galaxy and a possible BL Lac object;
- 1 star;
- 6 spectroscopically unclassified objects, 5 of which have a redshift determined mainly on the basis of a single emission line.

4.4 Notes on individual sources

Brief comments on the optical and/or radio properties are given for all the objects in Table 2 and for a few additional sources.

03–02 Bright early-type galaxy, in a group; the close-by galaxy at $\sim 12''$ north of the radio position has the same redshift.

05–03 The most likely identification ($L = 5.7$) is with a very faint galaxy, classified as *Early*, with a low S/N spectrum for which a redshift determination was not possible. It is likely to be a member of a compact group of galaxies, since other four objects are within $5''$. The brightest one ($L = 4.5$) has a tentative redshift of 0.165, but, due to its much brighter magnitude with respect to the other members of the group, it is more likely to be a foreground object.

Table 2. Spectroscopic Results

$N_{1.4}$	$N_{2.4}$	R	z	Emission Lines	$W_0[\text{OII}]$	D(4000)	Class	Class	Comment
				Measured	(\AA)		Spectral	Final	
03	02	17.1*	0.094	no		2.03	Early	Early	
05	03	22.03	?	no			Early?	Early	low S/N
06	--	16.9*	0.000	no			Star	Star	G6 type
07	04	20.60	?	no			BL Lac?	BL Lac?	
08	--	19.43	2.166	yes	Ly α , CIV, CIII]		AGN1	AGN1	x-ray source
09	05	17.65	0.165	no		2.06	Early	Early	
11	--	20.9*	0.368	yes	[OII], H β , [OIII], H α	50.8 \pm 8.1	Late(S)	Late(S)	
13	08	18.8*	0.229	yes	[OII], H β , [OIII]	51.3 \pm 1.3	Late(S)	Late(S)	
15	10	19.41	1.663	yes	CIV, CIII]		AGN1	AGN1	x-ray source
17	12	21.7*	1.147	yes	[OII]	18.5 \pm 0.8	Unclass.	Early	
18	--	19.2*	0.209	yes	[OII], H β , [OIII]	17.2 \pm 0.5	Late(S)	Late(S)	
20	15	22.12	\sim 0.7	no			Early?	Early	z from cluster
22	--	20.07	0.255	yes	[OII]	25.7 \pm 2.0	Late	Late	
24	--	20.02	0.280	yes	[OII], H β , [OIII]	40.5 \pm 7.1	Late(S)	Late(S)	
25	17	20.85	0.688	yes	[OII], [OIII]	18.7 \pm 0.7	AGN2	AGN2	Seyfert 2 gal.
26	19	20.05	0.551	no		>1.9	Early	Early	
27	20	17.10	0.217	no		2.04	Early	Early	
30	22	21.78	0.957	yes	MgII, [OII]	6.7 \pm 1.2	Unclass.	Early	x-ray source
31	23	21.58	0.757	no		1.64	Early	Early	
32	24	22.50	0.814	yes	[OII]	9.4 \pm 1.1	Unclass.	Early	
38	30	19.32	0.387	no		1.97	Early	Early	x-ray source
43	34	18.60	0.219	no		1.49	Early	Early	noisy spectr.
47	--	20.05	0.579	no		>2.1	Early	Early	
48	36	17.40	0.154	yes	[OII], H β , [OIII]	7.6 \pm 0.9	Late	Late	Bright Spiral
50	--	18.01	0.255	yes	[OII], H β , [OIII]	18.7 \pm 0.8	Late(S)	Late(S)	
51	38	21.90	?	no			Early?	Early	
52	39	22.70	1.259	yes	[OII]	111.4 \pm 9.7	Unclass.	Early	
53	40	21.45	0.809	yes	[OII]	28.4 \pm 2.0	Unclass.	Early	merging
55	--	18.22	0.276	yes	[OII], H α	6.9 \pm 0.4	Late?	Late?	
57	43	22.09	?	no			Unclass.	Late?	low S/N
60	46	21.15	0.702	no		2.02	Early	Early	
--	47	19.8*	0.275	yes	[OII], H α	11.0 \pm 1.6	Late?	Late?	
61	--	19.8*	2.110	yes	Ly α , CIV, CIII]		AGN1	AGN1	
63	--	20.2*	0.203	yes	[OII]	15.7 \pm 1.6	Late	Late	

06–00 Bright G star.

07–04 Blue object without any obvious spectral feature in its spectrum. Its colours ($U - B = -0.2$, $B - V = 0.56$, $V - R = 0.44$), together with its inverted radio spectrum ($\alpha_r = -0.42$), may suggest that this object is a BL Lac AGN. However, this identification has the lowest likelihood ratio in our sample ($L = 1.8$) because of its relatively large distance from the radio position (3.2 arcsec).

08–00 Broad-line quasar (Zitelli et al. 1992; MZZ7801), which is also X-ray emitter.

09–05 Bright early-type galaxy with radio emission probably powered by a mini-AGN in its nucleus, as suggested by its inverted radio spectrum ($\alpha_r = -0.68$).

11–00 Blue, emission-line galaxy with line ratios consistent with the lines being due to star-formation.

13–08 Emission-line galaxy with line ratios consistent with the lines being produced by a strong star-formation activity.

15–10 Broad-line quasar (MZZ5571), also X-ray emitter (Zamorani et al. in preparation).

17–12 High- z (1.147) galaxy, whose redshift determination is based on the presence of a single, relatively strong (EW=18.5 \AA) emission-line, identified with [OII] λ 3727.

18–00 Emission line galaxy with a starburst-like spectrum; the southern companion is at the same redshift and shows a late-type galaxy spectrum.

20–15 Faint, red galaxy surrounded by a number of galaxies with similar colours. It is likely to be at the center of a cluster. The cross-correlation analysis does not lead to any statistically significant redshift determination. The shape of the continuum at $\sim 8000 \text{\AA}$ suggests the possible presence of the CaH+K break at $z \sim 1.04$, but also this identification is not supported by any other emission or absorption line in the spectrum. For this reason, the redshift of this object has not been determined from its spectrum, but it has been tentatively estimated from the redshifts we measured

for three other cluster members ($z \simeq 0.7$). This object has an inverted radio spectrum ($\alpha_r = -0.24$). Due to its red colours, we classified this object as an *Early* galaxy.

22–00 Noisy spectrum, with only a relatively strong [OII] (EW=25.7 Å) but a quite reddened continuum; a brighter galaxy, 19'' south of the radio position has the same redshift.

24–00 Late-type spectrum galaxy with lines produced by strong star-formation activity.

25–17 Very red emission-line object classified as Seyfert 2 on the basis of its line-ratios, while its colours are more typical of an evolved elliptical/S0 galaxy. It has a companion at the same redshift within a few arcseconds, so that interaction could be partially responsible for the enhanced radio and line emission.

26–19 Early-type galaxy in a faint, inverted-spectrum ($\alpha_r = -0.11$) radio source.

27–20 Bright early-type galaxy at relatively low redshift ($z = 0.217$).

30–22 Triple radio source identified with a high redshift galaxy ($z = 0.957$), which is also an X-ray source. In the UV portion of the spectrum, some possible broad lines (MgII λ 2798 CII λ 2326) indicate the presence of an active nucleus, but the continuum shortward of 5500 Å is noisy and shows a suspect fall. Its colours are consistent with this object being an early-type galaxy. It is surrounded by other fainter objects, suggesting the presence of a group, but all of them are too faint for any redshift determination.

31–23 The faint early-type galaxy suggested as the most likely identification is the closest to the radio position. An equally faint, but bluer galaxy with strong [OII] at the same redshift is at 4.3 arcsec from the radio source. Other faint galaxies within a few arcsec suggest the presence of a group.

32–24 A compact group of faint galaxies coincides with the radio position. The more likely identification is with a high redshift galaxy ($z = 0.814$) showing a moderate [OII] emission-line in its spectrum. The colours are consistent with this object being an early-type galaxy.

38–30 Early-type galaxy coincident with the central component of a triple radio source, which is also an X-ray emitter.

43–34 Early-type spectrum galaxy (but noisy spectrum!) with a disk-like morphology. The spectrum is almost a straight line over the whole observed range and its shape is very similar to those of the young, reddened galaxies found by Hammer et al. (1997).

47–00 Early-type galaxy at the center of a small group at $z = 0.579$. The object at 5'' is a blue compact galaxy at the same redshift.

48–36 Bright spiral galaxy, spectrally classified as *Late*. Its line-ratios suggest current star-formation activity, although the spectrum is dominated by old stellar continuum.

49–37 A classical double radio source with no obvious optical identification. The CCD image suggests a possible association with a faint cluster.

50–00 Late-type spectrum galaxy, with line ratios consistent with the lines being due to star-formation activity.

51–38 Faint pair of sources, possibly forming a merging system. Despite a reasonable S/N in their spectra it was not possible to identify any obvious structure, nor obtaining a reliable redshift determination. Due to their red colours, this pair has been associated to the *Early* class.

52–39 Very faint, high- z (1.259) emission line galaxy,

whose redshift determination was based on a single, strong emission-line (EW = 111 Å), identified with [OII] λ 3727. The significant detection of continuum shortward of the line seems to exclude the Ly α hypothesis. The colours of this object, together with its radio and optical luminosities are consistent with it being a high- z elliptical galaxy.

53–40 Very faint, extremely red ($B - R > 3$) [OII] emitting galaxy at relatively high z (0.809). This is probably a close merging system, since its CCD image shows that it has two faint nuclei. Moreover, it is likely to be surrounded by a faint cluster. Due to its very red colours and to the inverted spectrum of its radio emission ($\alpha = -0.28$), it is likely to be an evolved object with a mini-AGN in its nucleus, whose radio and line emission are enhanced by the on-going merging.

55–00 Late-type, H α emitting galaxy with peculiar optical morphology. This is a very puzzling objects, since its distorted optical and radio morphologies strongly suggest this galaxy being in interaction with another close disk-galaxy (optical and radio tails connecting the two objects are clearly visible). However, their redshifts show a significant cosmological distance between them ($\Delta v = 6534$ km/s), which makes the suggested interaction rather unlikely. Moreover, the optical counterpart of the radio source has a close companion at the same redshift (at a distance of 6.1 arcsec).

56–42 This galaxy, although relatively bright ($R = 22.01$) and with a high likelihood ratio, has not been spectroscopically observed, since it was not in the area covered by the CCD exposures and was close to the detection limits of the photographic plates. However, it fell by chance in a 5 mins CCD frame taken during the last spectroscopic run, thus we could determine its magnitude and position.

57–43 Blue unclassified object. The spectrum shows two possible emission features (a large at ~ 8820 Å and a narrow at ~ 7250 Å) which we were not able to identify with any obvious spectral line. It is possible that one of the two lines be a spurious one, since it is a very low S/N spectrum. Due to its colours and spectral shape this object has been associated to the *Late* class.

58–44 The most likely identification for this object is a bright star, but, due to its likelihood ratio value < 1.5 we assumed it as a mis-identification.

60–46 Relatively high- z (0.702) early-type galaxy, possibly in a faint group: another object at 6.2'' has the same redshift and several fainter ones are within $\sim 8''$.

00–47 Late-type, H α emitting galaxy with a spectrum very similar to that of 55–00.

61–00 Broad-line quasar (MZZ8668).

63–00 Complex optical image constituted by two superimposed sources in the plates, whose redshifts ($z = 0.203$ and $z = 0.654$) show that they are not related. Both galaxies have emission line spectra, the most likely identification being with the galaxy at lower redshift and with moderate [OII] emission (EW = 15.7). The other galaxy is bluer, at higher redshift and with strong [OII] line (EW = 33.8).

5 RADIO AND OPTICAL PROPERTIES OF THE FAINT RADIO GALAXY POPULATION

Colour-redshift diagrams are presented in figure 3, while radio spectral index-radio flux, radio flux-optical magnitude,

magnitude–redshift and radio luminosity–absolute magnitude plots are presented in Figs 4a, b, c, and d. In both figures the objects are plotted with different symbols according to their spectral classification, while the spectrally unclassified galaxies are represented by a filled dot with either a circle or a square around, indicating colour classification from figure 3. The dashed lines in figure 4b represent different values of the radio–to–optical ratio R , defined as $R = S \times 10^{\frac{(m-12.5)}{2.5}}$, where S is the radio flux in mJy and m is the apparent magnitude.

For most objects the colours are consistent with their spectral classification (see fig. 3). The different classes of objects are discussed individually below.

5.1 Early–type galaxies

In this section we will consider in the group of early–type galaxies both those with redshift determination and those for which we were unable to measure the redshift (# 05–03, # 20–15 and # 51–38, plotted in the right side of figure 3), but with red colours consistent with those of the early–type class. The colour–redshift (figs. 3), magnitude–redshift (fig. 4c) and radio luminosity–absolute magnitude (fig. 4d) diagrams for our early–type objects (all the empty circles) are consistent with those expected for redshifted elliptical and S0 galaxies. The radio luminosities for all these galaxies are in the range $10^{23.0} < P_{1.4 \text{ GHz}} < 10^{24.8} \text{ W Hz}^{-1}$ ($H_0 = 50 \text{ km s}^{-1} \text{ Mpc}^{-1}$, $q_0 = 0.0$), consistent with them being Fanaroff–Riley I galaxies. Consistently with previous results, the early–type galaxies are the dominant population at $S > 1 \text{ mJy}$. However, at variance with what found by other authors (see, for example, Benn et al. 1993), we find a significant number of early–type galaxies also in the flux range $0.2 \leq S \leq 1 \text{ mJy}$. A more detailed discussion of the relative importance of different types of galaxies as a function of radio flux and optical magnitude will be given in section 6.

Below 2 mJy, about 13% of our radio sources have inverted radio spectrum (see figure 4a). Even if not all of them have been optically identified, it appears that most of these objects belong to the early–type class, in agreement with the results of Hammer et al. (1995), who found an even higher fraction of early–type galaxies with inverted radio spectra among their identified μJy radio sources ($S_{4.86 \text{ GHz}} > 16 \mu\text{Jy}$). The suggested presence of a low–luminosity AGN in the nuclei of these objects, responsible for the observed radio emission, applies also to the galaxies in our sample, which can be the “bright” counterpart of the Hammer et al. μJy sources (also with very faint optical magnitude, in the range $23 \lesssim V \lesssim 26$). Our non–inverted radio spectra early–type galaxies are probably powered by an active nucleus, too, since they all have absolute magnitude greater than $M_R = -21.5$ and relatively high radio luminosity and other plausible sources of radio emission (HII regions, planetary nebulae, supernova remnants) cannot account for the observed radio luminosity in galaxies brighter than this magnitude (Sadler, Jenkins & Kotany 1989; Rees 1978; Blanford & Rees 1978).

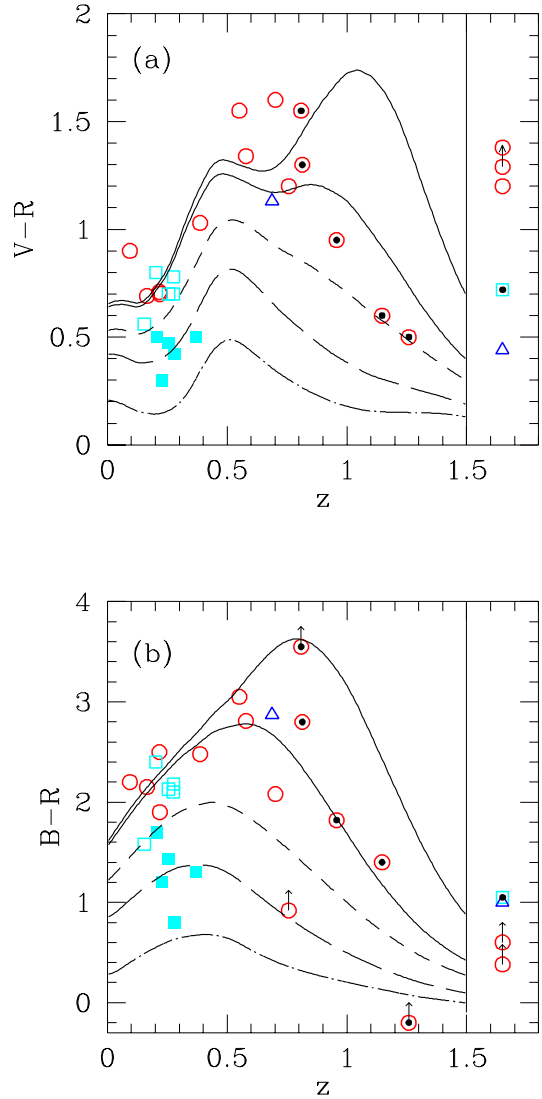


Figure 3. $V - R$ (a) and $B - R$ (b) colour versus redshift for the extragalactic identifications. The three quasars at $z > 1.5$ are not shown. The different symbols represent the different classes of objects: the empty circles stand for *Early* galaxies, the squares for *Late* galaxies (empty for normal and filled for star–forming galaxies), the empty triangles for AGNs (the type 2 Seyfert galaxy and the possible BL Lac object) and the filled dots for spectrally unclassified objects. The latter have either a circle or a square around the dot, indicating classification from these diagrams. At the right side of these figures also the colours for objects without redshift determination are plotted. The different curves correspond to the colour–redshift relations for galaxies derived from Bruzual & Charlot (1993) models and represent two different models for elliptical galaxies (solid lines), Sab–Sbc spirals (dashed line), Scd–Sdm spirals (long dashed line) and starburst galaxies (dotted–dashed line). The parameters of these models are given in Table 3 in Pozzetti et al. (1996).

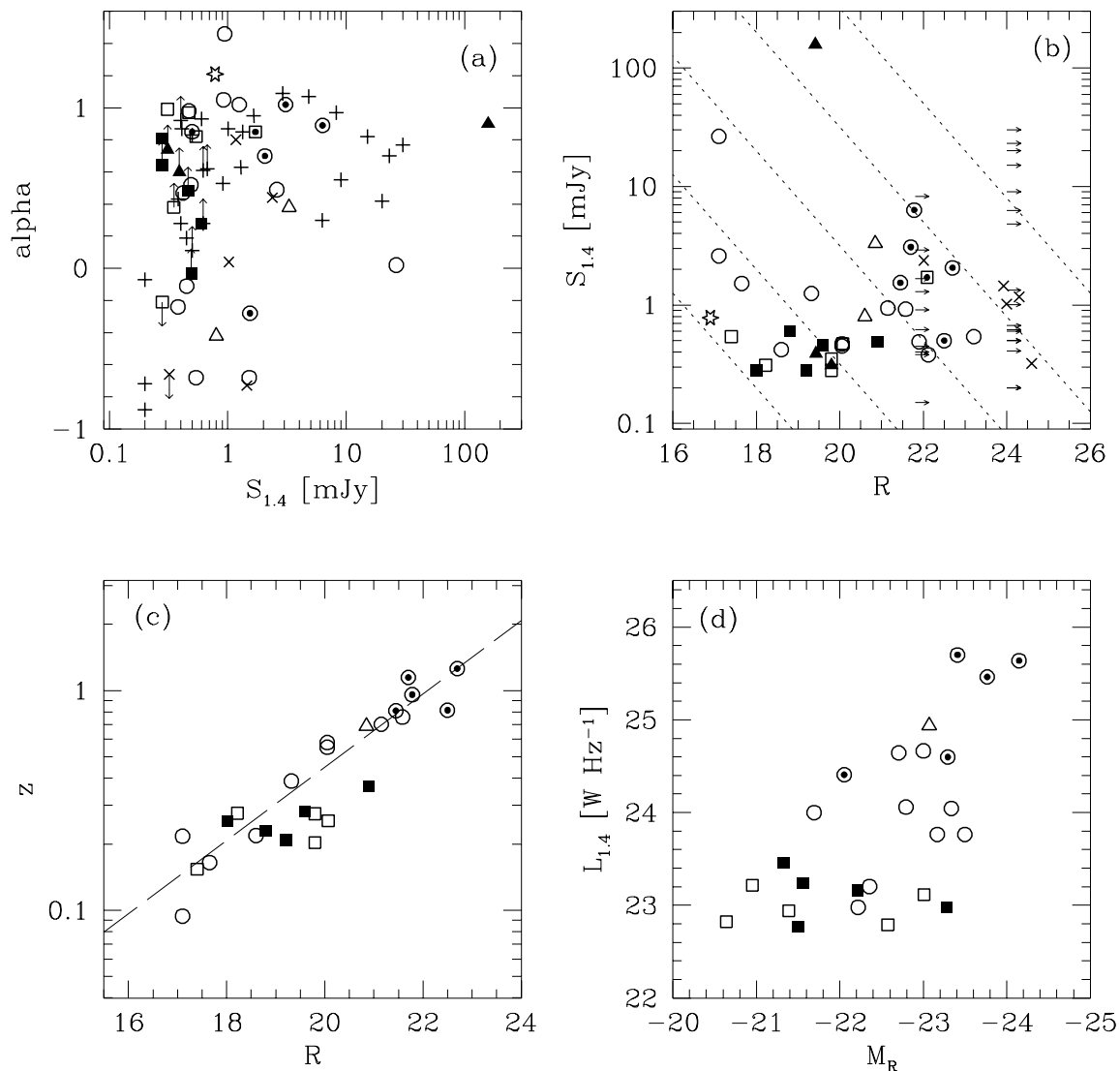


Figure 4. Radio spectral index vs. radio flux (a) and radio flux vs. R magnitude (b) for all radio sources. Symbols are the same as in figure 3, with the addition of filled triangles for quasars, an empty star for the star, diagonal crosses for objects with optical ID but no spectrum and vertical crosses for empty fields (arrows in panel b). The dotted lines in panel b are different radio-to-optical ratios, corresponding to $\log R = 1.5, 2.5, 3.5, 4.5, 5.5$. Redshift vs. R magnitude (c) and radio luminosity vs. absolute R magnitude (d) for the identifications. The dashed line in panel c is the best-fit R - z relation for *Early* galaxies in the sample.

5.2 Late-type and Star-forming Galaxies

Figures 3 and 4 show that late-type and star-forming galaxies occupy a narrow range at low-moderate redshift ($0.15 < z < 0.4$) and most of them have relatively bright apparent magnitudes ($R < 21.0$, $B < 22.5$), faint radio fluxes ($S_{1.4 \text{ GHz}} < 1$ mJy) and relatively low radio luminosities ($L_{1.4 \text{ GHz}} < 10^{23.5}$ W Hz $^{-1}$). All the galaxies classified as *Late(S)* (i.e. with significant star formation) on the basis of their spectra have blue colours, consistent with those of late spirals. The galaxies classified as *Late* are, instead, redder and some of them (# 55-00, # 00-47 and # 63-00) have

colours close to the locus expected for elliptical galaxies. Despite of this, we will keep for them the spectral classification.

Our *Late(S)* galaxies are part of the starburst population at low/intermediate redshift found in almost all the published sub-mJy identification works (e.g. Windhorst et al. 1985; Benn et al. 1993), whose radio and optical properties they fully resemble. Also their radio spectral indices (which are all steep, see fig. 4a) are consistent with their radio emission being due to synchrotron emission from supernova remnants, the main source of radio emission at 1.4 GHz in starburst galaxies, with typical spectral index in the

range $0.5 - 0.9$ ($S_\nu \propto \nu^{-\alpha}$). The radio luminosity of these star-forming galaxies occupy the range $10^{22.7} < L_{1.4 \text{ GHz}} < 10^{23.5} \text{ W Hz}^{-1}$, similar to (but narrower than) that found by Benn et al. (1993) for their starburst objects. The *Late* galaxies occupy about the same range of radio and optical luminosities and all but one of them have steep radio spectral indices.

The blue unclassified object # 57-43 has been associated to the *Late* class, due to its colour properties. However, the radio flux and the apparent magnitude of this object are out of the ranges occupied by all the other *Late* galaxies in our sample. So, its classification remains quite uncertain.

5.3 AGNs

Three objects (# 08-00, # 15-10 and # 61-00) have broad emission lines and are in the MZZ quasar sample (Zitelli et al. 1992). They are the highest redshift objects in our sample ($z = 2.166, 1.663$ and 2.110 respectively) and their absolute optical magnitudes range from -25.9 to -27.2 , all brighter than the limit $M_B = -23$ often used to separate Seyferts and quasars. They are probably hosted by elliptical galaxies, though only one of them (15-10, which is also the brightest radio source in our sample) can be defined as radio-loud on the basis of the ratio between the radio and optical luminosities (Gruppioni and Zamorani, in preparation). Their radio powers are in the range $10^{25.3} - 10^{27.8} \text{ W Hz}^{-1}$, comparable to those of lower redshift 3CR and 5C quasars.

One object (# 25-17) has only narrow lines and was classified Seyfert 2 on the basis of its emission line ratios. The radio and optical properties of this object resemble those of the high redshift radio galaxies in our sample (described in the following section). In fact, its radio luminosity is $10^{24.9} \text{ W Hz}^{-1}$, well inside the range occupied by our high- z galaxies, and its colours, as well, are as red as those of evolved ellipticals.

5.4 High-redshift Emission-Line Galaxies

The group of 5 galaxies at relatively large redshifts ($z > 0.8$) whose spectra were left unclassified in section 4.3 is composed by intrinsically powerful radio sources. Their radio powers occupy the range $10^{24.4} < L_{1.4 \text{ GHz}} < 10^{25.7} \text{ W Hz}^{-1}$. In this range of radio powers, far too high for classical late-type and star-forming galaxies, Fanaroff-Riley class I and class II radio galaxies (FRI and FR II) coexist in roughly equal numbers (Zirbel and Baum 1995). All these five radio-galaxies are close to the dividing line between FRI and FR II galaxies in the radio luminosity-absolute magnitude plane (see, for example, Ledlow and Owen 1996). At the relatively poor angular resolution of our radio data, a morphological classification is not possible: three of them are unresolved with a typical upper limit to the size of a few arcsec, one consists of a slightly resolved single component, one (# 30-22) is a triple radio source, which, however, does not resemble the classical FR II double radio sources, since the three components are not aligned with each other.

Thus, our higher redshift and more powerful radio sources are very unlikely to be star-forming galaxies as they would have been classified on the basis of their emission

lines (in most cases just one emission line associated with [OII]). Four out of five of these galaxies have $\text{EW}([\text{OII}])$ in the range $6-28 \text{ \AA}$, the only exception being # 52-39, which has an EW larger than 100 \AA . Since at the magnitudes and redshifts of these galaxies 80% of the field galaxies have $\text{EW}([\text{OII}]) > 15 \text{ \AA}$ (Hammer et al. 1997), we conclude that the star formation in these galaxies is not particularly strong. This would be even more true if some, if not most, of the emission line flux were due not to stellar but to nuclear ionization. The relatively low [OII] emission would be consistent with these radiogalaxies belonging to the FRI class, with # 52-39 being the only good candidate for an FR II classification. In fact, for a given absolute magnitude, line luminosity in FR II radiogalaxies is significantly higher than in FRI galaxies, while the latter have only slightly higher line luminosity than normal “radio quiet” elliptical galaxies (Zirbel and Baum 1995).

Figure 3 shows that the colours for these five galaxies are reasonably consistent with those expected at their redshift for early type galaxies (ellipticals or early spirals), while they are significantly redder than those expected for late type spirals or starburst-dominated galaxies. For this reason, and taking into account also the continuity with the other early-type galaxies at lower redshift in the redshift-magnitude plane (figure 4c) and their relatively high radio luminosity (figure 4d), we are confident that, despite the presence of [OII] emission in their spectra, they are physically unrelated to the star-forming galaxies identified at low-moderate redshift.

However, we can not exclude that some of these red galaxies at relatively high redshift ($z > 0.8$) are highly obscured galaxies, similar to the heavily reddened starbursts at $z \leq 1$ recently detected in the mid/far-infrared by ISO and in the sub-mm by SCUBA (Hammer & Flores 1998; Lilly et al. 1998). These objects, showing star formation rates, derived from infrared data, in excess of $100 M_\odot \text{ yr}^{-1}$ are far from being classical star-forming galaxies. Similarly to our red radio sources, they have red colours and relatively faint [OII] emission lines (Hammer et al. 1995). At variance with our high redshift red galaxies, however, they have smaller radio-to-optical ratios.

5.5 Radio sources without identification

For 6 radio sources we have likely optical counterparts, but no spectroscopic data. Five of them (# 00-06, # 21-16, # 36-27, # 41-32 and # 45-00) are at the limit of our CCD exposures ($R \sim 24$ and $B \sim 25$), while one (# 56-42), at the limit of our plates, has $R \sim 22$. Twenty-eight additional radio sources have no optical counterpart either in the plates (9 objects, $R \geq 21.8$) or in the CCD data (19 objects, $R \geq 24$). The location of these objects in the radio flux - optical magnitude plane is shown in figure 4b (crosses and arrows). Fourteen of these objects have $S > 1 \text{ mJy}$, while 14 have $S < 1 \text{ mJy}$; most of them have steep radio spectra ($\alpha > 0.5$). Figure 4b shows that almost all these objects have a radio to optical ratio significantly higher than that typical of late type galaxies, including those with significant star-formation. We therefore conclude that most of them are likely to be associated with early-type galaxies. This is consistent with the fact that early-type galaxies constitute the large majority of the identifications with objects

fainter than $B \sim 22.5$. In the following discussion we will focus only on the sample of 19 radio sources without reliable optical counterpart on CCD data. Under the assumption that our unidentified objects are early-type galaxies, we used the $z-R$ magnitude relation defined by the objects in figure 4c, and other similar relations from larger samples (Vigotti, private communications, for a sample which contains data for about 100 3CR and B3 radiogalaxies) to estimate their expected redshifts. The redshift – magnitude relation in the R band has a significantly larger scatter than the similar relation in K band, because the R band, probing the UV rest-frame luminosity, where a large intrinsic scatter in high- z radiogalaxies is present (Dunlop et al. 1989), is more affected by possible AGN contamination, recent star formation or dust. For this reason, given an optical magnitude, only a relatively large redshift range rather than a true redshift can be estimated. For the magnitude corresponding to the limits in the CCD data, this range turns out to be $1.2 \lesssim z \lesssim 3.0$. The corresponding radio luminosities would be in the range $\log P_{1.4 \text{ GHz}} = 25.6 \pm 0.6$ at $z \sim 2$.

Of course, we can not exclude that a few of the unidentified radio sources are, instead, associated to starburst galaxies. If so, however, they should be really extreme objects in terms of their ratio between radio and optical luminosities. With just one exception (# 57-43, whose association with the *Late* class is rather uncertain (see Section 4.4)), all the late-type galaxies in our sample have $1.5 \lesssim \log R \lesssim 3.0$, while all but one of the unidentified radio sources have $\log R \gtrsim 3.3$. Radio observations of large and complete samples of spiral galaxies show that the fraction of such galaxies with $\log R$ higher than this value is $< 10^{-3}$ (Condon 1980; see also Hummel 1981). Given the number of galaxies with $R \leq 22$ in the entire area covered by our radio data (~ 5400), and assuming that 50% of them can be considered part of the starburst class, we can qualitatively estimate that the number of such galaxies which could have been detected with $\log R \geq 3.3$ is at most of the order of a few (i.e. < 3). Obviously, this argument *assumes* that the radio-to-optical ratio for starburst galaxies does not undergo a strong evolution with redshift at $z \gtrsim 1$.

In any case, to shed light on the nature of our unidentified radio sources deeper optical observations would be needed, but if they indeed are high- z radio galaxies the best observing band would be in the near infrared, where both the K-correction effects and the dispersion in the redshift-magnitude relation are much smaller than in the optical.

6 DISCUSSION

In previous works it has been shown that the optically brighter part of the radio source population at sub-mJy level is composed largely of starburst galaxies at relatively low redshifts. Although these results were based on small fraction of spectroscopic identifications (Benn et al. 1993), it has often been unduly assumed that they could still be true for the entire population of sub-mJy radio sources.

Our data, based on a significantly higher fraction of optical identifications (close to 50%) although on a relatively small sample of radio sources, do not support this assumption. In fact, we find that early-type galaxies (including the high- z emission-line galaxies, which are probably the

faint end of the more powerful elliptical radio galaxy population like the 3CR) are $(44 \pm 16)\%$ of all the radio sources fainter than 1 mJy identified with galaxies in our sample. In the same radio flux interval Benn et al. found a dominance of blue narrow emission line galaxies and a percentage of early-type galaxies of only about 8% (7/84 early-type against 76/84 star-forming galaxies!). The reason of this discrepancy is very likely to be ascribed to the deeper optical magnitude reached in our identification work with respect to the previous ones ($B \simeq 24$ to be compared with $B \simeq 22.3$ of Benn et al. 1993). In fact, our sample suggests an abrupt increase in the fraction of identifications with early-type galaxies at around $B \simeq 22.5$, which is just above the magnitude limit of the Benn et al. sample (see figure 4b). Dividing the sub-mJy sample in two sub-samples (brighter and fainter than $B = 22.5$), the fraction of early-type galaxies with respect to the total number of radio sources spectroscopically identified with galaxies increases from $(9 \pm 9)\%$, in good agreement with the Benn et al. results in the same magnitude range, to about 100%.

Moreover if, as discussed in Section 5.5, also most of the unidentified radio sources are likely to be associated with high redshift elliptical radio galaxies, the total fraction of early-type galaxies in our sub-mJy sample can be estimated to be of the order of $(60 - 70)\%$. This fraction is in good agreement with the prediction of the model for the evolution of faint radio sources developed by Rowan-Robinson et al. (1993). Integrating the radio luminosity functions of spiral galaxies, derived from the Benn et al. sample, and elliptical galaxies (Dunlop and Peacock 1990) and testing various models for the evolutionary laws of the spiral luminosity function, they indeed find that ellipticals still contribute about 60% of the integrated counts to a radio limit of 0.1 mJy. Previous models for the interpretation of the sub-mJy radio counts, based on older luminosity functions and different models for the evolution, predicted a substantially lower fraction of early type galaxies in the same flux range (see, for example, Danese et al. 1987).

Although the percentages of early and late type galaxies we estimated from our data are in agreement with the predictions of the Rowan-Robinson et al. models, the redshift distribution of our sample of late type galaxies (all of them with $z < 0.4$) appears not to be consistent with the predictions of the same models, in which a not negligible tail of high redshift galaxies is expected (see figure 6 in Rowan-Robinson et al. 1993). Although with relatively large errors, because of the small size of our sample, the “local” volume-densities of our late type galaxies are consistent with the radio luminosity function of spiral galaxies computed by Rowan-Robinson et al. (1993). If our conclusion that most of the unidentified radio sources are likely to be associated with high redshift elliptical radio galaxies is correct, this would imply a smaller amount of evolution for the radio luminosity function of late type galaxies than that assumed in Rowan-Robinson et al. models. Alternatively, agreement with Rowan-Robinson et al. models could be obtained only if a significant fraction of our unidentified radio sources were instead to be classified as starburst galaxies. If actually placed at the high redshift predicted by these models, their radio powers, in the range $10^{24} - 10^{25} \text{ W Hz}^{-1}$, would require unplausibly high star formation rates, in excess of a few thousand $M_{\odot} \text{ yr}^{-1}$, on the basis of the relation

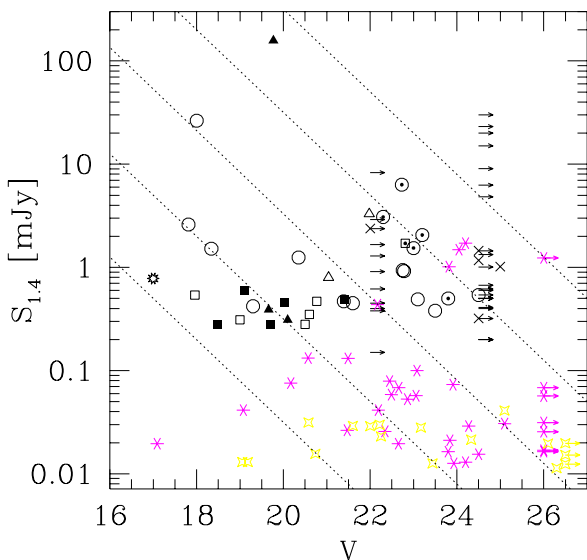


Figure 5. 1.4 GHz flux vs. V magnitude for our identifications (symbols as in fig. 3) and for Hammer et al. (1995) and Windhorst et al. (1995) counterparts of μ Jy sources (represented, respectively, by asterisks and diagonal crosses). The 1.4 GHz fluxes for the Windhorst et al. objects have been obtained assuming the median spectral index of the Hammer et al. sample ($\alpha_{med} = 0.2$). The thick arrows at $V = 26.0$ are the lower limits of Hammer et al., while the thick arrows at $V = 26.5$ are the lower limits of Windhorst et al. The dotted lines correspond to the same radio-to-optical ratios as in figure 4b.

between star formation rate and non-thermal radio emission (Condon 1992). Moreover, their radio-to-optical ratios, significantly higher than those of brighter late type galaxies, would suggest a radio emission mechanism different from that of local starburst galaxies, probably not directly related to the star formation episodes. In any case, larger and fainter samples of identifications would be needed in order to choose between these alternatives.

In this respect, it is interesting to compare our results at sub-mJy level with the existing data at μ Jy level, where the preliminary identification results obtained for the very few existing samples (Hammer et al. 1995; Windhorst et al. 1995; Richards et al. 1998) are still somewhat unclear. These papers have shown that the population of μ Jy radio sources is made of star forming galaxies, ellipticals and AGNs. Given the faint magnitude of the optical counterparts, the exact fraction of each category is not well defined yet.

In figure 5 we show the 1.4 GHz flux versus V magnitude for our data and the Hammer et al. and Windhorst et al. ones (for which V magnitudes are available). The 1.4 GHz fluxes have been computed using the 1.5–5 GHz spectral indices reported by Hammer et al. for their objects and assuming the median value of the Hammer et al. spectral index distribution ($\alpha_{med} = 0.2$) for the Windhorst et al. ones. The dotted lines correspond to the same radio-to-optical ratios as in figure 4b. The figure shows that the fraction of radio sources with large radio-to-optical ratios, typical of the

more powerful radio sources, decreases in the μ Jy samples. For $\log R > 3.5$ this fraction is larger than 50% (37/68) in our sample, while it is smaller than 35% (17/51) for the μ Jy samples. Vice versa, most of the μ Jy radio sources have the same radio-to-optical ratio as our low redshift star-forming and elliptical galaxies.

7 CONCLUSIONS

Optical identifications down to $R \sim 24$ have been performed for a sample of 68 radio sources brighter than 0.2 mJy at 1.4 or 2.4 GHz. About 60% of the radio sample have a likely optical counterpart on deep CCD exposures or ESO plates. Even in the CCD data, reaching $R \sim 24$ and $B \sim 25$, 19 out of 50 sources are not identified. Spectra have been obtained for 34 optical counterparts brighter than $R \simeq 23.5$. The spectra provided enough information to determine object type and redshift in most cases (29 objects). This percentage of spectroscopic identifications is the highest obtained so far for radio sources in this radio flux range. The objects are a mixture of classical early-type galaxies (E/S0), with no detectable emission lines, covering the redshift range 0.1–0.8, star-forming and late-type galaxies at moderate redshifts ($z < 0.4$), emission-line galaxies at relatively high z (> 0.8) and AGNs. The star-forming galaxies are very similar in colour, luminosity and spectral properties to those found in other sub-mJy surveys (i.e. Benn et al. 1993). Contrary to previous results, star-forming galaxies do not constitute the main population in our identification sample. In fact, even at sub-mJy level the majority of our radio sources are identified with early-type galaxies. This apparent discrepancy with previous results is due to the fainter magnitude limit reached in our spectroscopic identifications. In fact, the fraction of sub-mJy early-type galaxies in our sample abruptly increases around $B \simeq 22.5$, which is approximately the magnitude limit reached by previous identification works. Moreover, the high- z emission-line galaxies have spectra, colours, and absolute magnitudes similar to those of the classical bright elliptical radio galaxies found in surveys carried out at higher radio fluxes. Their radio luminosity ($10^{24.4} < L_{1.4 \text{ GHz}} < 10^{25.7} \text{ W Hz}^{-1}$), far too high for classical star-forming galaxies, is in the range where FRI and FRII radiogalaxies coexist in roughly equal number. These objects are therefore likely to constitute the faint radio luminosity end of the distant elliptical radio galaxy population, thus further increasing the fraction of early-type galaxies in our identified sample. Moreover, using mainly the large radio-to-optical ratio and the information from the available limits on the optical magnitudes of the unidentified radio sources, we conclude that the great majority of them are likely to be early-type galaxies, at $z > 1$. Our classification for these faint objects can be tested with photometric and spectroscopic observations in the near infrared. If correct, it would suggest that the evolution of the radio luminosity function of spiral galaxies, including starbursts, might not be as strong as suggested in previous evolutionary models.

8 ACKNOWLEDGEMENTS

Support for this work was provided by ASI (Italian Space Agency) through contracts 95-RS-152 and ARS-96-70.

REFERENCES

- Baldwin I.A., Phillips M.M. & Terlevich R., 1981, *PASP*, 93, 5
- Benn C.R., Rowan-Robinson M., McMahon R.G., Broadhurst T.J. & Lawrence A., 1993, *MNRAS*, 263, 98
- Bertin E., Arnouts S., 1996, *A&AS*, 117, 393
- Blanford R.D. & Rees M.J., 1978, *Phys. Scripta*, 17, 265
- Bruzual G., 1983, *ApJ*, 273, 105
- Bruzual G. & Charlot S., 1993, *ApJ*, 405, 538
- Condon J.J., 1980, *ApJ*, 242, 894
- Condon J.J., 1984, *ApJ*, 287, 461
- Condon J.J., 1989, *ApJ*, 338, 13
- Condon J.J., 1992, *ARA&A*, 30, 575
- Condon J.J. & Mitchell K.J., 1984, *AJ*, 89, 610
- Danese L., Franceschini A., Toffolatti L., De Zotti G., 1987, *ApJL*, 318, L15
- Dunlop J.S., Guiderdoni B., Rocca-Volmerange B., Peacock J.A. & Longair M.S., 1989, *MNRAS*, 240, 257
- Dunlop J.S., Peacock J.A., 1990, *MNRAS*, 247, 19
- Enard D., and Delabre B., 1982, *SPIE* 445, 552.
- Franceschini A., Danese L., De Zotti G. & Xu C., 1988, *MNRAS*, 233, 175
- Grupponi C., Zamorani G., de Ruiter H.R., Parma P., Mignoli M. & Lari C., 1997, *MNRAS*, 286, 470
- Hammer F., Crampton D., Lilly S.J., Le Fèvre O. & Kenet T., 1995, *MNRAS*, 276, 1085
- Hammer F., Flores H., Lilly S., Crampton D., Le Fèvre O., Rola C., Mallen G., Schade D., Tresse L., 1997, *ApJ*, 481, 49
- Hammer F. & Flores H., 1998, in T.X. Thuan, C. Balkowski, V. Cyatte & J.T.t. Van eds., *Dwarf Galaxies and Cosmology*, Editions Frontières, Gif-sur-Yvette, in press (astro-ph/9806184)
- Horne K., 1986, *PASP*, 98, 609
- Hummel E., 1981, *A&A*, 93, 93
- Kinney A.L., Calzetti D., Bohlin R.C., McQuade K., Storchi-Bergmann T., Schmitt H.R., 1996, *ApJ*, 467, 38
- Koo D.C., Kron R.G., 1982, *A&A*, 105, 107
- Kron R.G., 1980, *ApJS*, 43, 305
- Kron R.G., Koo D.C. & Windhorst R.A., 1985, *A&A*, 146, 38
- Ledlow M.J. & Owen F.N., 1996, *AJ*, 112, 9L
- Le Fèvre O., Hudon D., Lilly S.J., Crampton D., Hammer F. & Tresse L., 1996, *ApJ*, 461, 534
- Lilly S.J., Eales S.A., Gear W.K., Bond J.R., Dunne L., Hammer F., Le Fèvre O., Crampton D., 1998, in B. Kaldeich ed., *NGST: Science and Technological Challenges*, ESA Publication Division, ESTEC, in press (astro-ph/9807261)
- Marano B., Zamorani G. & Zitelli V., 1988, *MNRAS*, 232, 111
- Mignoli M., 1997, *Mem.SAI*, 68, 335
- Pozzetti L., Bruzual G. & Zamorani G., 1996, *MNRAS*, 281, 953
- Rees M.J., 1978, *Phys. Scripta*, 17, 193
- Richards E.A., Kellermann K.I., Fomalont E.B., Windhorst R.A. & Partridge R.B., 1998, *ApJ*, submitted (astro-ph/9803343)
- Rola C.S., Terlevich E. & Terlevich R.J., 1997, *MNRAS*, 289, 419
- Rowan-Robinson M., Benn C.R., Lawrence A., McMahon R.G. & Broadhurst T.J., 1993, *MNRAS*, 263, 123
- Sadler E.M., Jenkins C.R. & Kotany C.G., 1989, *MNRAS*, 240, 591
- Sutherland W. & Saunders W., 1992, *MNRAS*, 259, 413
- Thuan T.X. & Condon J.J., 1987, *ApJL*, 322, L9
- Wall J.V., Benn C.R., Grueff G. & Vigotti M., 1986, in Swings J.P., ed., *Highlights of Astronomy Vol. 7*. Reidel, Dordrecht, p. 345
- Windhorst R.A., 1984, PhD Thesis, Univ. of Leiden
- Windhorst R.A., Dressler A. & Koo D.C., 1987, in Hewitt A., Burbidge G. & Fang L.Z., eds, *Observational Cosmology*. Reidel, Dordrecht, p. 573
- Windhorst R.A., Fomalont E.B., Kellermann K.I., Partridge R.B., Richards E., Franklin B.E., Pascarelle S.M. & Griffiths R.E., 1995, *Nature*, 375, 471
- Windhorst R.A., Miley G.K., Owen F.N., Kron R.G. & Koo D.C., 1985, *ApJ*, 289, 494
- Zitelli V., Mignoli M., Zamorani G., Marano B. & Boyle B.J., 1992, *MNRAS*, 256, 349
- Zirbel E.L. & Baum S.A., 1995, *ApJ*, 448, 521

This figure "fig2_1.gif" is available in "gif" format from:

<http://arxiv.org/ps/astro-ph/9811309v1>

This figure "fig2_2.gif" is available in "gif" format from:

<http://arxiv.org/ps/astro-ph/9811309v1>

This figure "fig2_3.gif" is available in "gif" format from:

<http://arxiv.org/ps/astro-ph/9811309v1>

This figure "fig2_4.gif" is available in "gif" format from:

<http://arxiv.org/ps/astro-ph/9811309v1>

This figure "fig2_5.gif" is available in "gif" format from:

<http://arxiv.org/ps/astro-ph/9811309v1>

This figure "fig2_6.gif" is available in "gif" format from:

<http://arxiv.org/ps/astro-ph/9811309v1>